Numerical control of two-dimensional shock waves in dual solution domain by instant temperature disturbances

A. K. Alekseev[1] and I. M. Navon[2,*,†]

[1]*Moscow Institute of Physics and Technology, Moscow 141700, Russia*
[2]*School of Computational Science, Florida State University, Tallahassee, FL 32306-4120, USA*

SUMMARY

The search for the temperature disturbance causing transition between regular and Mach reflections in the dual solution domain is addressed in an optimization statement. The gradient of the discrepancy between the current and target flow fields was calculated using adjoint equations. The control was determined by gradient-based optimization. The flow field simulation is verified via a posteriori error estimates using the solution of an additional adjoint problem. Copyright © 2012 John Wiley & Sons, Ltd.

1. INTRODUCTION

Both the numerical simulation of high speed flows with an interaction of shock waves and the control of such flows are of significant current theoretical and practical interest. There are many techniques for an aerodynamic flow control at high speeds based on different ways of energy deposition [1–3]. The flow parameter domains where the solution is not unique are of special interest from the viewpoint of control efficiency. The coexistence of two stable flow modes under the same conditions provides attractive prospects for controls because the support of selected mode past transition is not necessary. We consider, herein, one of the well known bistable flow patterns. At the intersection of two symmetric shock waves, there exists the range of Mach numbers and shock slopes where both the regular and Mach reflections exist, for example, see References [4, 5]. Several works [6–10] considered triggering in the dual solution domain using various disturbances of flow parameters. The transition from the regular reflection to Mach mode was obtained in [6] and investigated from the standpoint of minimal control energy. Shock waves caused by the energy deposition at the edge surface were studied. The transition from the Mach to regular reflection was achieved in [7] by the numerical simulation of the injection of cold gas jet that occupies total Mach stem zone. The paper in [8] considered both experimentally and computationally the influence of impulse laser heat deposition on the flow field near shock crossing. The influence of energy impulse was imitated in computations by an initial temperature variation. The computations provided the transition from Mach to regular modes, while the experiments demonstrated some reduction of Mach stem height with its consequent recovery to the original magnitude. The similar results were reported by Yan *et al.* [9]. The paper in [10] states the impossibility of transition from the Mach to regular mode under any energy deposition control.

---

*Correspondence to: Michael Navon, Department of Scientific Computing, Florida State University, Tallahassee, FL 32306-4120, USA.
†E-mail: inavon@fsu.edu

The search for controls on a base of qualitative and intuitive assumptions is the common feature of approaches described in [6–10]. It seems to be expedient to enrich these methods by some quantitative technique. The present paper concerns the search for triggering disturbances using an inverse problem in the optimization statement. We address the control of transition from the Mach to regular mode and vice versa by an instant energy deposition. This deposition is imitated by the spatially distributed temperature disturbance $\Delta T_0(x, y)$ applied to the steady flow. The sensitivity of the flow pattern to this disturbance is calculated using the adjoint problem. The controls are computed using the gradient based optimization.

The approximation error affects significantly the transition from Mach to regular reflection and causes qualitative differences in results of computation, compare References [5] and [10]. Herein, we estimate the time relaxation and approximation errors for pointwise density past shock intersection using a posteriori approach based on adjoint problem according to References [11, 12].

2. SHOCK WAVE INTERSECTION SIMULATION

The interaction of the plain supersonic flows engendered by the couple of symmetric edges is the main subject of the present consideration. The flow simulation is performed using 2D+1 Euler equations

$$\frac{\partial \rho}{\partial t} + \frac{\partial (\rho U_k)}{\partial x^k} = 0; \tag{1}$$

$$\frac{\partial (\rho U_i)}{\partial t} + \frac{\partial (\rho U_k U_i + P \delta_{ik})}{\partial x^k} = 0; \tag{2}$$

$$\frac{\partial (\rho E)}{\partial t} + \frac{\partial (\rho U_k h_0)}{\partial x^k} = 0; \tag{3}$$

with initial conditions

$$\rho_0(x, y), U_0(x, y), V_0(x, y), T_0(x, y). \tag{4}$$

The latter variable ($T_0(x, y)$) may be disturbed if the follow control is applied.

Calculations are conducted in the domain $\Omega = (0 < x < X_{\max}, 0 < y < Y_{\max})$ and time interval $(0 < t < t_f)$.

Here, $U_1 = U, U_2 = V$ are the velocity components, $h_0 = (U^2 + V^2)/2 + h$, $h = (\gamma/\gamma - 1)(P/\rho) = \gamma e$, $e = RT/\gamma - 1$, $E = (e + (1/2)(U^2 + V^2))$ are enthalpies and energies (per unit volume), $P = \rho RT$ is the state equation and $\gamma = 1.4$ is the specific heat ratio.

At the left boundary ($x = 0$) we accept the inflow conditions before and past two oblique shock waves. On the lateral boundaries ($y = 0, y = Y_{\max}$) we impose inflow conditions past shocks at the initial part ($0 < x < X_{\text{raref}}$) and conditions imitating flow past an expansion fan on the remaining boundary part ($X_{\text{raref}} < x < X_{\max}$). The rarefaction part of flow causes the acceleration in 'a liquid Laval nozzle' to reach supersonic velocities that provide the existence of considered flow pattern and significantly facilitate the statement of outflow boundary condition at $x = X_{\max}$. The flow structure for both considered modes is presented in Figures 1 and 2.

The Euler equations were solved by methods of the second and fourth orders of accuracy over the space. The MUSCL (Monotone Upstream-centered Schemes for Conservation Laws) [13] method with the numerical fluxes calculated via HLLC (Harten, Lax, van Leer, Einfeldt, with contact correction) [14] or method by Sun and Katayama [15] were used as the second-order solver. The fourth-order method by Yamamoto and Daiguji [16] was used in the main part of optimization tests.

At numerical tests the nonunique solution was searched for freestream Mach numbers 3.45–6 and flow deflection angles $\Theta \in (19°, 30°)$. Figure 3 presents the bifurcation diagram (theoretical and numerical) on the plane (M, Θ). Calculations conducted on different grids (100×100, 400×400) by the methods of second and fourth orders of approximation are provided in this figure in comparison with the theoretical data from [5]. Numerical results for the transition from the regular shock
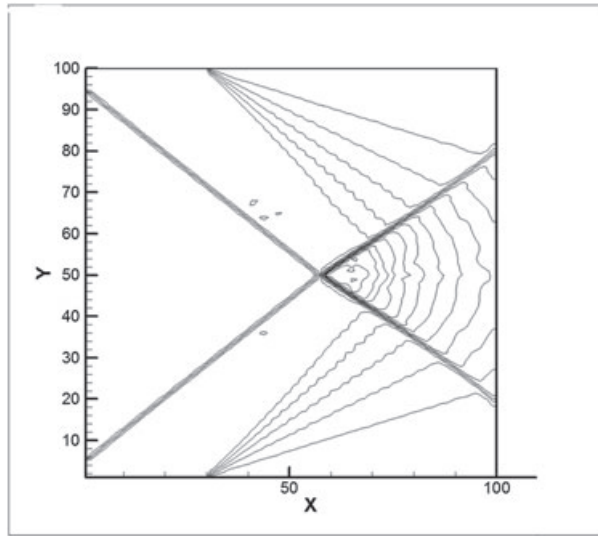
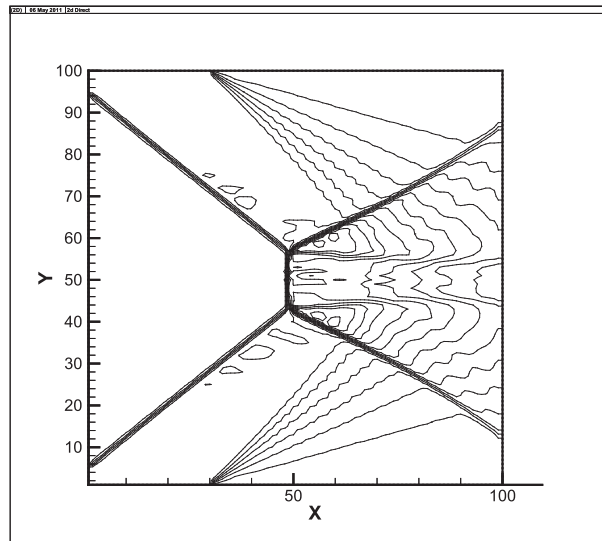Figure 1. Density isolines. Regular reflection.

Figure 2. Density isolines. Mach reflection.

reflection to Mach mode present good coincidence with the theory, while the transition from the Mach mode to regular one is modeled with the significant error. Similar results were obtained in [5] and attributed to the small height of Mach stem that is specific for this transition. The increasing of approximation order seems to be more useful from the accuracy viewpoint in comparison with the mesh refining (in the range of 100–400 nodes over one coordinate) when transition from Mach to regular mode is simulated. On the other hand, the transition from the regular to Mach reflection weakly depends on number of nodes and a bit more apparently on the order of approximation.

The influence of approximation error is reported in [5] as the reason for difficulties in the simulation of both the shock interaction and the flow response to control disturbances. Herein, the error of the density $\varepsilon = \rho^{\text{est}} = \int_{\Omega} \rho(x)\delta(x - x^{\text{est}})\mathrm{d}\Omega$ at a reference point past shock crossing was used as an accuracy criterion. According [17] the variation of the density (considered as a goal functional) in dependence on the local truncation error may be presented as follows:

$$\delta\varepsilon = \delta\rho^{\text{est}} = \iint\limits_{\Omega} \left(\delta\rho\,\Psi_\rho + \delta U\,\Psi_U + \delta V\,\Psi_V + \delta h\,\Psi_h\right)\mathrm{d}\Omega. \tag{5}$$
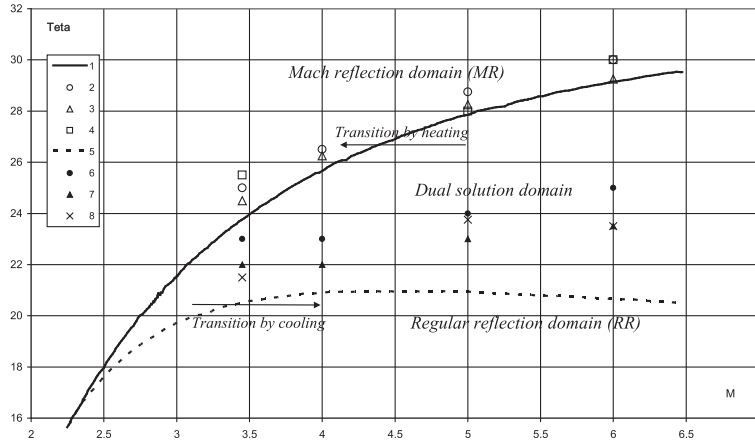
Figure 3. Hysteresis curve of transition between Mach and regular modes in dependence on freestream Mach number and flow deflection angle. 1 – upper branch ($RR \rightarrow MR$, detachment criterion); 2 – upper branch (second order, 100×100); 3 – upper branch (fourth order, 100×100); 4 – upper branch (second order, 400×400); 5 – lower branch ($MR \rightarrow RR$, von Neumann criterion); 6 – lower branch (second order, 100×100); 7 – lower branch (fourth order, 100×100); and 8 – lower branch (second order, 400×400).

Herein, the adjoint variables $\Psi_\rho, \Psi_{U^i}, \Psi_e$ are taken from the solution of the following adjoint problem [11, 17]:

$$\frac{\partial \Psi_\rho}{\partial t} + \frac{\partial \Psi_i}{\partial t} U^i + \frac{\partial \Psi_e}{\partial t} E + U^k \frac{\partial \Psi_\rho}{\partial x^k} + U^k U^i \frac{\partial \Psi_i}{\partial x^k} + (\gamma - 1) \frac{\partial \Psi_k}{\partial x^k} e + U^k h_0 \frac{\partial \Psi_e}{\partial x^k} - \delta \left(x^{k,\text{est}} - x^k \right) = 0$$

$$\frac{\partial \Psi_i}{\partial t} \rho + \frac{\partial \Psi_e}{\partial t} \rho U^i + U^i \frac{\partial \Psi_k}{\partial x^k} + U^i \frac{\partial \Psi_i}{\partial x^k} + \frac{\partial \Psi_\rho}{\partial x^k} + h_0 \frac{\partial \Psi_e}{\partial x^k} + U^i U^k \frac{\partial \Psi_e}{\partial x^i} = 0 \qquad (6)$$

$$\frac{\partial \Psi_e}{\partial t} + \gamma U^k \frac{\partial \Psi_e}{\partial x^k} + (\gamma - 1) \frac{\partial \Psi_k}{\partial x^k} = 0$$

initial conditions: $\Psi_{\rho,U^i,e}\big|_{t=0} = 0$;
boundary conditions: $\Psi_{\rho,U^i,e}\big|_{\partial\Omega=0} = 0$.
The algorithm [18] is used for this problem solving.
The expression

$$\delta\varepsilon_c = \sum_{k,n}^{N,Nx} \left(\Psi_{\rho;n,k}\delta\eta_{\rho;n,k} + \Psi_{U;n,k}\delta\eta_{U;n,k} + \Psi_{V;n,k}\delta\eta_{V;n,k} + \Psi_{h;n,k}\delta\eta_{h;n,k} \right) h_x h_y \qquad (7)$$

is used as the discrete form of (5). The values $\delta\eta_{f;n,k}$ approximate the local truncation error and are obtained by the action of the high (fourth) order finite difference stencil on the numerically computed flow field. For example, for density component we use the expression

$$\eta_{\rho;n,k} = \frac{-F_{\rho,n,k+2} + 8F_{\rho,n,k+1} - 8F_{\rho,n,k-1} + F_{\rho,n,k-2}}{12h_x}$$
$$+ \frac{-\Theta_{\rho,n+2,k} + 8\Theta_{\rho,n+1,k} - 8\Theta_{\rho,n-1,k} + \Theta_{\rho,n-2,k}}{12h_y} \qquad (8)$$

where $F^n_{\rho;k,n} = (\rho U)_{nk}$ and $\Theta^n_{\rho;k,n} = (\rho V)_{nk}$.

The comparison of the error density distribution $\Psi_{\rho;n,k}\delta\eta_{\rho;n,k} + \Psi_{U;n,k}\delta\eta_{U;n,k} + \Psi_{V;n,k}\delta\eta_{V;n,k} + \Psi_{h;n,k}\delta\eta_{h;n,k}$ over the flow field for schemes of the second and fourth orders of accuracy is presented in Figures 4 and 5. Despite the maximum amplitude of error density being greater for the fourth-order method, the error itself (because of averaging over all flow fields (7)) is much smaller (0.0055 instead of 0.03). Although the effective order of approximation of both schemes (with nominal
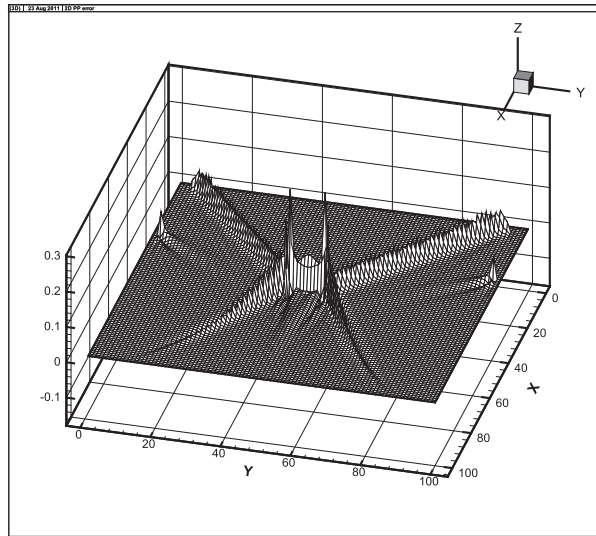
Figure 4. Error density distribution for scheme of the second-order of accuracy.
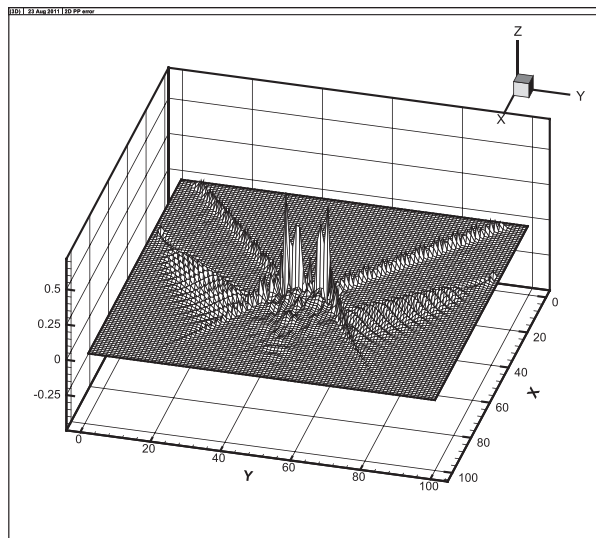

Figure 5. Error density distribution for scheme of the fourth-order of accuracy.

second and fourth orders) in the presence of shock waves is about (or less) than unit [19, 20], the higher order approximation is more accurate.

For Mach configuration, the maximums of error density are located in the vicinity of triple points (see Figures 4 and 5) and are much greater than the errors both at the oblique and normal shocks. As far as the Mach stem height decreases, zones of significant errors approach each other, which causes a rapid increase of average error in the vicinity of the Mach stem. This feature of error density behavior may be the reason for the low accuracy of computations for short Mach stems (at lower curve of Figure 3) as reported in [5] and observed in the present paper. In contrast to triple point, the points of two oblique shocks' crossing exhibit the moderate error growth (Figures 6 and 7).

The absolute value of the density error at the reference point (at the plane of symmetry on outflow boundary) was not greater, 0.02 for the regular mode and 0.03 for Mach shock intersection. The temporal relaxation error was also estimated a posteriori using the approach in [21]. For the same
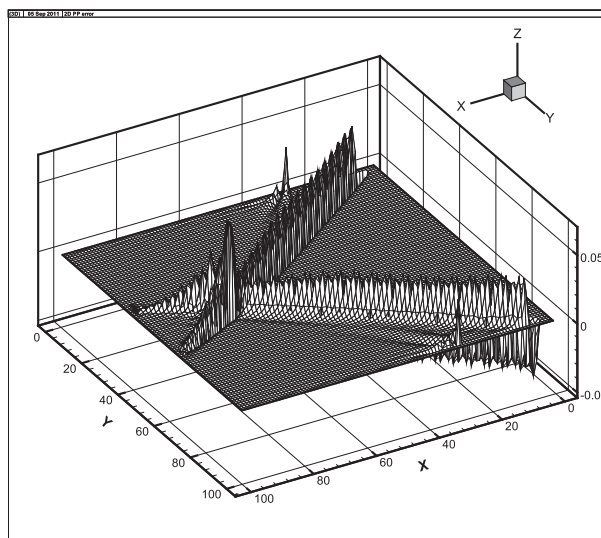
Figure 6. Error density distribution for scheme of the second-order of accuracy.
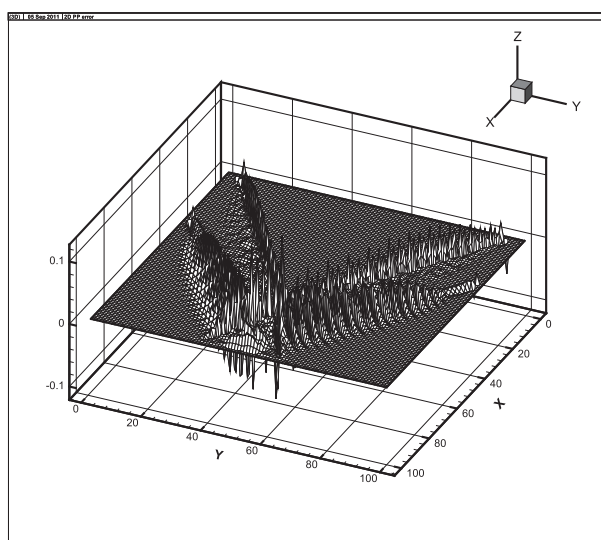

Figure 7. Error density distribution for scheme of the fourth-order of accuracy.

point this error was kept less than the spatial approximation error by several orders of magnitude via the selection of long enough relaxation time t_f.

3. OPTIMAL CONTROL PROBLEM

We consider the functional

$$\varepsilon(T_0) = 1/2 \sum_m \int_\Omega \left(f_m(t, x, y) - f_m^{\text{aim}}(x, y) \right)^2 \mathrm{d}\Omega + \alpha/2 \int_\Omega \left(\Delta T_0(x, y) \right)^2 \mathrm{d}\Omega \tag{9}$$

presenting the mismatch of computed $f_m(t, x, y)$ and target $f_m^{\text{aim}}(x, y)$ flow parameters (in tests presented below only the density $\rho^{\text{aim}}(x, y)$ is used for $f_m^{\text{aim}}(x, y)$). The disturbance of temperature $\Delta T_0(x, y)$ at the initial time is used as a control variable. The velocities and density are assumed

to be not changed at this time. The latter penalty term ensures the search for controls of minimum norm; however, it deteriorates the convergence. The regularization parameter α should be chosen as a compromise between the disturbance minimum and the convergence of iterations.

The gradient of functional (9) regarding the temperature disturbance may be expressed as

$$\nabla \varepsilon_{T_0(x,y)} = \Psi_e(0, x, y) + \alpha \Delta T_0(x, y). \tag{10}$$

Herein, Ψ_e is obtained from the solution of the following adjoint system:

$$\frac{\partial \Psi_\rho}{\partial t} + \frac{\partial \Psi_i}{\partial t} U^i + \frac{\partial \Psi_e}{\partial t} E + U^k \frac{\partial \Psi_\rho}{\partial x^k} + U^k U^i \frac{\partial \Psi_i}{\partial x^k} + (\gamma - 1) \frac{\partial \Psi_k}{\partial x^k} e + U^k h_0 \frac{\partial \Psi_e}{\partial x^k} - (\rho - \rho^{\text{aim}}) = 0 \tag{11}$$

$$\frac{\partial \Psi_i}{\partial t} \rho + \frac{\partial \Psi_e}{\partial t} \rho U^i + U^i \frac{\partial \Psi_k}{\partial x^i} + U^i \frac{\partial \Psi_i}{\partial x^k} + \frac{\partial \Psi_\rho}{\partial x^k} + h_0 \frac{\partial \Psi_e}{\partial x^k} + U^i U^k \frac{\partial \Psi_e}{\partial x^i} - (U^i - U^{i,\text{aim}}) = 0 \tag{12}$$

$$\frac{\partial \Psi_e}{\partial t} + \gamma U^k \frac{\partial \Psi_e}{\partial x^k} + (\gamma - 1) \frac{\partial \Psi_k}{\partial x^k} - (E - E^{\text{aim}}) = 0. \tag{13}$$

$$\begin{aligned} \text{initial conditions} \;\; &\Psi_{\rho, U^i, e}\big|_{t=0} = 0; \\ \text{boundary conditions:} \;\; &\Psi_{\rho, U^i, e}\big|_{\partial \Omega = 0} = 0. \end{aligned} \tag{14}$$

This system differs from Equation (6) only by the source terms and is solved by the same method [18].

The conjugate gradients method $T_0^{n+1}(x, y) = T_0^n(x, y) - \tau S(\nabla \varepsilon_{T_0})$ is used starting from the undisturbed field $T_0(x, y)$. Every iteration involves solving both the forward and adjoint problem. The flow field variables $f_m(t, x, y)$ are used in coefficients at the adjoint problem solving. A certain number of the temporal slices (10–20) was saved to account for a time dependence of the flow variables. The flow parameters at current time were determined via the linear interpolation between the slices. Despite the close accuracy, the calculations by the second-order solver on the grid 400×400 needed greater computational time by about two orders of magnitude if compared with the fourth order. Therefore, the optimization was performed using fourth-order method on the grid 100×100.

Numerical tests demonstrate the feasibility of transition from the regular to Mach mode under a spatially distributed temperature disturbance for all tested Mach numbers and reverse transition for small Mach numbers. Past 10–15 iterations, the discrepancy (9) has diminished from two to four orders of magnitude. Calculations were performed in the range of Mach number M and flow deflection Θ angles belonging to the dual solution domain. The regularization parameter α was varied from zero to a certain maximum value, which did not prevent from a convergence. The total time of computation for inverse problem solving is about 20–30 greater if compared with the single flow field calculation.

Figures 8–10 present controls for freestream Mach number 3.45 (the temperature disturbance is normed by the undisturbed freestream temperature). Figure 8 demonstrates the temperature disturbance providing transition from the regular (Figure 1) to Mach (Figure 2) intersection The regularization parameter α equals zero and the relative norm of the disturbance $\|\Delta T_0\|_{L_2(\Omega)} / \|T_0\|_{L_2(\Omega)}$ is equal to 0.6. Its sign is positive (heating) in the main part of the field. For the regularization parameter $\alpha = 10$ (the higher acceptable value from the viewpoint of convergence) the norm of disturbance equals 0.26 and its shape (Figure 9) is very close to one of the solution without regularization (Figure 8).

Figure 10 presents the temperature disturbance that is sufficient for the transition from the Mach to regular mode. The relative norm of disturbance is equal to 0.3 (no regularization). Its sign is negative (cooling), which correlates with the results on feasibility to control this transition by the cold gas injection [7].
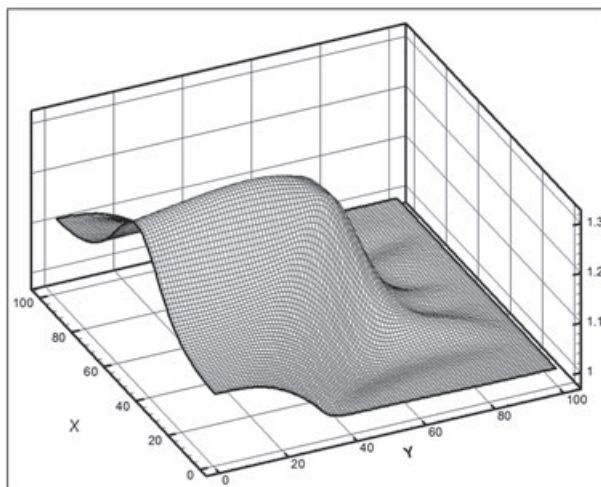
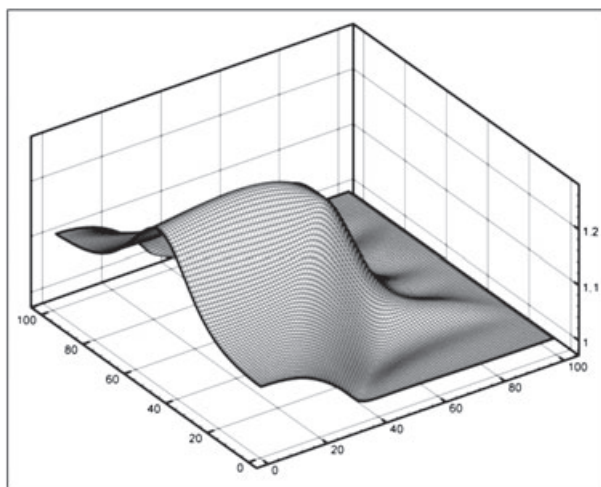Figure 8. Temperature disturbance causing regular to Mach transition.

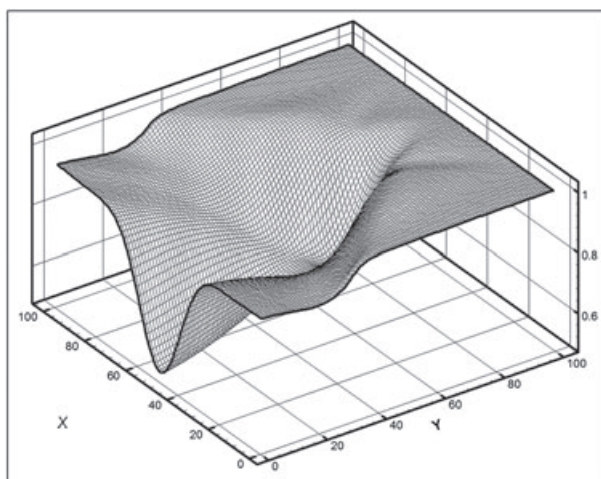Figure 9. Temperature disturbance causing regular to Mach transition (regularized result).

Figure 10. Temperature disturbance causing Mach to regular transition.

In presented results the goal functional was formed as the discrepancy of density in current and target states. For other sets of flow parameters, which may be used in the functional (9), similar results are obtained.

In general, the considered method enables finding a control disturbance for the transition from the regular to Mach mode ($RR \rightarrow MR$) in the freestream Mach range 3.45–6. This control corresponds to an energy deposition. The Mach to regular transition ($MR \rightarrow RR$) can be forced for $M = 3.45$ by cooling. The attempts to obtain Mach to regular transition for $M > 3.5$ failed. During iterations, controls move to a negative absolute temperature. These results correlate with the form of the low branch (von Neumann criterion) of the bifurcation diagram (Figure 3) if the Mach number dependence on the temperature is accounted.

4. DISCUSSION

In general, the flow discontinuities (shocks, shift layers) may forbid the gradient optimization based on adjoint equations. However, there are papers successfully dealing with the minimization of shock action by a shape control (see, e.g., [12]). These results suggest that the shocks in flow field may not cause discontinuities in a control variables space. Similarly, the above presented results on the gradient-based optimization demonstrate the existence of smooth paths in the space of controls (temperature disturbances) that connect two steady shock patterns. The failure of temperature control for the transition from the Mach to regular reflection may be explained by the shape of bifurcation curve and is not connected with flow field discontinuities.

However, the considered approach is limited by relatively small disturbances, which do not cause a total alteration of the flow structure. It is not unlikely that nonlinear strong disturbances may provide additional paths in the control variable space to implement the considered triggering.

The selection of $\Delta T_0(x, y)$ as the control variables confines the analysis to the set of relatively powerful energy sources. The more general controls via time dependent heat sources $Q(x, y, t)$ belonging to the space of higher dimension may provide a more complicated behavior, and are above the scope of the present paper.

The results on temperature control that are qualitatively consistent with the shape of the bifurcation curve verify the considered approach and hold the promise for using it for other, less transparent, physical actions (mass injection, dynamical effects, etc) [2, 22, 23]

It is difficult at present to offer the technique for the generation of the necessary temperature disturbance. However, the development of different ways of energy deposition including above laser heating, the glow charge and microwave heating [3, 24] offers the prospect of progress in this direction.

5. CONCLUSION

A posteriori error estimation provides both the quantitative (pointwise error) and qualitative (error density distribution) information on the results of numerical simulation.

According the numerical computations, the transition from the regular to Mach shock reflection may be stimulated by the positive temperature disturbance. This result presents certain prospects for controls of this transition by an energy deposition.

The transition from the Mach to regular shock reflection may be triggered by the negative temperature disturbance for relatively small freestream Mach numbers ($M < 3.5$). For $M > 3.5$ the numerical experiments fails to find any control. These results demonstrate the impossibility of $MR \rightarrow RR$ transition by any energy deposition.

The adjoint-based gradient optimization enables the systematic search for the control of shock wave interaction at the moderate increase of computing time if compared with a simple flow field calculation.

The adjoint equations used for the inverse problem solving are practically identical to equations used for a posteriori error estimation that promise a significant saving of efforts in coding and debugging.

REFERENCES

1. Knight D, Kuchinskiy V, Kuranov A, Sheikin E. *Survey of Aerodynamic Flow Control at High Speed By Energy Deposition*. AIAA Paper 2003-0525, (2003).
2. Ghosh Sh, Manesh K. Numerical simulation of the fluid dynamic effects of laser energy deposition in air. *Journal of Fluid Mechanics* 2008; **605**:329–354.
3. Knight DD, Kolesnichenko YF, Brovkin V, Khmara D. High speed flow control using microwave energy deposition. *16th Australasian Fluid Mechanics Conference*, Crown Plaza, Gold Coast, Australia, 2-7 December 2007; 199–207.
4. Ivanov MS *et al.* The reflection of asymmetric shock waves in steady flows: a numerical investigation. *Journal of Fluid Mechanics* 2002; **469**:71–87.
5. Ivanov MS, Vandromme D, Fomin VM, Kudryavtsev AN, Hadjadj A, Khotyanovsky DV. Transition between regular and Mach reflection of shock waves: new numerical and experimental results. *Shock Waves* 2001; **11**:199–207.
6. Mouton CA, Hornung HG. Experiments on the mechanism of inducing transition between regular and Mach reflection. *Physics of Fluids* 2008; **20**:126103-1–126103-11.
7. Kudryavtsev AN, Khotyanovsky DV, Ivanov MS, Hadjadj A, Vandromme D. Numerical investigations of transition between regular and Mach reflections caused by free-stream disturbances. *Shock Waves* 2002; **12**:157–165.
8. Yan H, Adelgren R, Elliott G, Knight D, Beutner T, Ivanov M. *Laser Energy Deposition in Intersecting Shocks*. AIAA Paper 2002–2729.
9. Yan H, Adelgrenm R, Elliott G, Knight D, Beutner T. Effect of energy addition on MR$RR transition. *Shock Waves* 2003; **13**(2):113–121.
10. Khotyanovsky DV, Kudryavtsev A, Ivanov MS. Effects of a single-pulse energy deposition on steady shock wave reflection. *Shock Waves* 2006; **15**:353–362.
11. Marchuk GI. *Adjoint Equations and Analysis of Complex Systems*. Kluwer Academic Publishers: Dordrecht, Hardbound, 1995; 484.
12. Nadarajah SK, Jameson A, Alonso J. *An Adjoint Method for the Calculation of Remote Sensitivities in Supersonic Flow*. American Institute of Aeronautics and Astronautics Paper Paper -2002-0261.
13. van Leer B. Towards the ultimate conservative difference scheme. V. A second-order sequel to Godunov's method. *J. Comput. Phys.* 1979; **32**:101–136.
14. Toro EF. *Riemann Solvers and Numerical Methods for Fluid Dynamics*. Springer Verlag: Berlin, 2009; 724.
15. Sun M, Katayama K. An artificially upstream flux vector splitting for the Euler equations. *Journal of Computational Physics* 2003; **189**:305–329.
16. Yamamoto S, Daiguji H. Higher-order-accurate upwind schemes for solving the compressible Euler and Navier-Stokes equations. *Computers and Fluids* 1993; **22**:259–270.
17. Alekseev AK, Navon IM. A posteriori error estimation by postprocessor independent of flowfield calculation method. *Computers & Mathematics with Applications* 2006; **51**:397–404.
18. Toro E, Siviglia A. PRICE: Primitive centered schemes for hyperbolic system of equations. *Int. Journal for Numerical Methods in Fluids* 2003; **42**:1263–1291.
19. Carpenter MH, Casper JH. Accuracy of shock capturing in two spatial dimensions. *AIAA J* 1999; **37**(9):1072–1079.
20. Gallouet T, Herard J-M, Seguin N. Some recent finite volume schemes to compute Euler equations using real gas EOS. *Int. Journal for Numerical Methods in Fluids* 2002; **39**(12):1073–1138.
21. Alekseev AK, Navon IM. Estimation of goal functional error arising from iterative solution of Euler equations. *International Journal of Computational Fluid Dynamics* April–May 2008; **22**(4):221–228.
22. Bisek NJ, Boyd ID, Poggie J. Numerical study of plasma-assisted aerodynamic control for hypersonic vehicles. *J. of Spacecraft and Rockets* 2009; **46**(3):568–576.
23. Shang JS, Huang PG, Yan H, Surzhikov ST, Gaitonde DV. *Hypersonic Flow Control Utilizing Electromagnetic-Aerodynamic Interaction*, American Institute of Aeronautics and Astronautics Paper 2008-2606, Dayton OH, April 2008.
24. Surzhikov ST, Shang JS. *Plasmadynamics of Glow Discharge in Hypersonic Internal Flows*, American Institute of Aeronautics and Astronautics Paper Paper 2007-0994, Reno NV, January 2007.